JACS
JOURNAL OF THE AMERICAN CHEMICAL SOCIETY
pubs.acs.org/JACS
Article

Fluorescent Biosensor for Measuring Ras Activity in Living Cells

Ryan Weeks, Xin Zhou, Tina L. Yuan, and Jin Zhang*

Cite This: J. Am. Chem. Soc. 2022, 144, 17432−17440
Read Online
ACCESS | Metrics & More | Article Recommendations | Supporting Information

ABSTRACT: The small GTPase Ras is a critical regulator of cell growth and proliferation. Its activity is frequently dysregulated in cancers, prompting decades of work to pharmacologically target Ras. Understanding Ras biology and developing effective Ras therapeutics both require probing Ras activity in its native context, yet tools to measure its activities in cellulo are limited. Here, we developed a ratiometric Ras activity reporter (RasAR) that provides quantitative measurement of Ras activity in living cells with high spatiotemporal resolution. We demonstrated that RasAR can probe live-cell activities of all the primary isoforms of Ras. Given that the functional roles of different isoforms of Ras are intimately linked to their subcellular distribution and regulation, we interrogated the spatiotemporal regulation of Ras utilizing subcellularly targeted RasAR and uncovered the role of Src kinase as an upstream regulator to inhibit HRas. Furthermore, we showed that RasAR enables capture of KRasG12C inhibition dynamics in living cells upon treatment with KRasG12C covalent inhibitors, including ARS1620, Sotorasib, and Adagrasib. We found in living cells a residual Ras activity lingers for hours in the presence of these inhibitors. Together, RasAR represents a powerful molecular tool to enable live-cell interrogation of Ras activity and facilitate the development of Ras inhibitors.

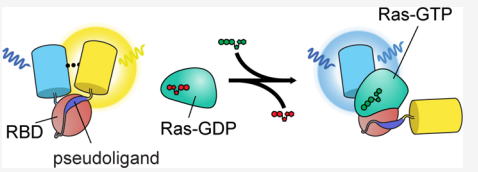

Downloaded via TSINGHUA UNIV on November 5, 2022 at 06:56:34 (UTC).
See https://pubs.acs.org/sharingguidelines for options on how to legitimately share published articles.

INTRODUCTION

As a small GTPase, Ras regulates cell growth and proliferation by acting as a molecular switch downstream of growth factor receptors.[1] Like all GTPases, Ras is a guanine nucleotide binding protein and regulated by guanine exchange factors (GEFs) and GTPase activating proteins (GAPs).[2] GTP-bound Ras has an effector binding region poised for high-affinity interactions with downstream effectors such as Raf,[3] which result in propagation of signaling. While Ras signaling is canonically initiated from the plasma membrane, it has become increasingly clear that the spatiotemporal dynamics of Ras are complex, and that functional roles of different isoforms of Ras are tightly coupled with their subcellular distribution and regulation.[4,5] Ras mutations are prevalent in cancers, and targeting mutant Ras has been a priority in cancer therapy for decades.[6,7] Although it was once considered "undruggable", pioneering work on K-RasG12C inhibitors[8−11] elicited a substantial amount of excitement and extensive efforts in the field of anti-Ras therapy and eventually led to the FDA-approved breakthrough therapy for the treatment of patients with locally advanced or metastatic non-small cell lung cancer with KrasG12C mutation.[12] Given that KRasG12C inhibitors target a mere fraction of potential oncogenic Ras targets, development of new anti-Ras therapy is still extensively pursued. Both understanding the spatiotemporal regulation of Ras and development of new anti-Ras therapy require probing Ras activity in its native context. To measure the activity of Ras, researchers have traditionally relied on Ras pulldown assays, which utilize the Ras binding domain (RBD) of Raf1 to enrich active Ras from cell lysates followed by Western Blot analysis. This method suffers from poor spatiotemporal resolution, is difficult to scale to high throughput, and essentially removes the target from its native context.[13] Therefore, there is an urgent need to develop live-cell Ras activity assays.

Genetically encoded fluorescent biosensors have emerged as powerful tools for investigating the spatiotemporal regulation of signaling molecules in living systems. In the context of drug development, live-cell assays can provide quantitative, real-time assessment of target engagement within native biological contexts,[14] which better mimic the disease setting than in vitro assays and allow for assessment of drug properties such as permeability and stability. Many Ras biosensors have been previously developed and can be classified into two types: translocation-based and ratiometric, Förster resonance energy transfer (FRET)-based. Translocation-based biosensors track the spatiotemporal dynamics of Ras activity through translocation of a cytosolically localized RBD, fused to a fluorescent protein, to compartments of Ras activity.[15] This approach was used in early studies to report the presence of Ras activity at the Golgi Apparatus.[16,17] However, the subcellular localization of these biosensors could be influenced by multiple factors and signal quantitation is prone to artifacts from variations in cell thickness and probe expression levels, which may have contributed to some controversial observations.[16,18,19] On

Received: May 16, 2022
Published: September 19, 2022

© 2022 American Chemical Society

https://doi.org/10.1021/jacs.2c05203
J. Am. Chem. Soc. 2022, 144, 17432−17440

the other hand, current FRET-based Raichu biosensors contain full-length Ras and the RBD of Raf1 coupled to fluorescent protein FRET pairs; activation of Ras within the sensor drives Ras-RBD interaction, leading to an increase in FRET.[20] While Raichu and other biosensors with similar designs[21,22] allow for more reliable quantitation, they entail heterologous expression of modified Ras as part of the biosensor and essentially serve as GEF/GAP biosensors, as the measurements rely on the activity of cellular GEFs and GAPs. To provide reliable, quantitative measurements of cellular Ras activity, new Ras biosensor designs are required. Here, we report the development and characterization of a new biosensor enabling direct Ras activity measurements. Using this biosensor, we provide new mechanistic insights into the regulation of HRas by Src kinase and demonstrate the utility of this biosensor in a live-cell Ras inhibitor assay.

RESULTS

Design and Validation of RasAR. To develop a biosensor capable of quantitative measurement of cellular Ras activity, we utilized the RBD from Raf1 as the sensing component and sought to translate a binding event to a conformational change by employing a pseudoligand design.[22] We derived a pseudoligand from the effector binding region of Ras, using a crystal structure of active Ras bound to Raf1 RBD[23] as a blueprint. GTP binding to Ras triggers a conformational change that allows the effector binding region of Ras to bind to the effector RBD. Peptides derived from this region have been shown to bind RBD with low affinity.[24] We chose the pseudoligand sequence QNHFVDEYDPTI based on its ability to bind RBD in an appropriate orientation to poise a fluorescent protein pair that can undergo FRET (Figure S1a). The Raf1 RBD and pseudoligand were joined by a linker and sandwiched between a pair of fluorescent proteins, mCerulean3 and YPet (Figure 1a,b). A nuclear export signal (NES) was also attached to the C-terminus of the construct to promote cytosolic localization (Figure 1b). In the absence of Ras, the pseudoligand engages the RBD, bringing the fluorescent proteins into proximity to promote FRET. Binding of active Ras to the RBD displaces the pseudoligand, leading to a decrease in FRET (Figure 1a).

To test for proper functionality, we co-expressed the biosensor, which we named Ras Activity Reporter (RasAR), with KRasWT, constitutively active (CA) KRasQ61L or KRasG12C, or dominant negative (DN) KRasS17N, each N-terminally fused to mCherry, in COS-7 cells. As shown in Figure 1c,d, cells expressing KRasQ61L or G12C exhibited significantly higher cyan-over-yellow (C/Y) emission ratios than cells expressing KRasWT or S17N, suggesting higher Ras activity in Q61L- or G12C-expressing cells. For instance, a higher emission ratio was observed for KRasQ61L compared with the DN mutant KRasS17N (n = 1077 and 873 cells for mCherry-KRasQ61L and mCherry-KRasS17N, respectively, Cohen's d = 2.19; Supplementary Table 1). Incorporating an R89L mutation, which is known to substantially disrupt Ras binding,[25] within the biosensor RBD substantially reduced the emission ratio differences (Figure 1d, Cohen's f = 0.15 for RasAR(R89L), f = 0.84 for RasAR). The observed differences in the biosensor C/Y emission ratio were not caused by variations in overexpression of Ras wildtype or mutants, as C/Y emission ratios were elevated across varying mCherry intensities (Figure S1b,c). In addition to differences in the C/Y emission ratio, the biosensor subcellular localization varied

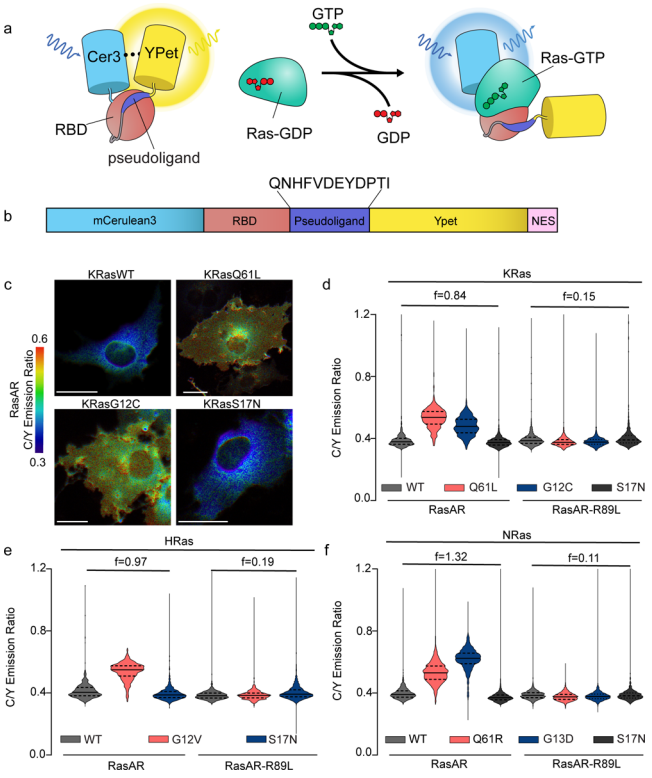

Figure 1. RasAR provides quantitative measurement of live-cell activities of all the primary isoforms of Ras. Design (a) and domain structure (b) of RasAR, which contains the Ras binding domain (RBD) derived from Raf1 and a pseudoligand designed from the effector binding region of Ras sandwiched between the FRET pair mCerulean3 and YPet. Ras binding to RasAR displaces the pseudoligand and leads to a decrease in FRET between mCerulean and YPet. (c) Representative pseudocolor images of the cyan-over-yellow (C/Y) emission ratios from COS-7 cells co-expressing RasAR along with different variants of mCherry-KRas. Warmer colors correspond to higher ratios and thus higher Ras activity. Co-expression with KRasWT or the dominant negative S17N mutant shows lower activity and cytosolic localization in comparison to the constitutively active Q61L or G12C mutants. Scale bars, 25 μm. Images are representative of three independent experiments. (d–f) C/Y emission ratios of COS-7 cells expressing RasAR or RasAR-(R89L) along with mCherry-labeled variants of KRas (d), HRas (e), or NRas (f). Data are combined from three independent experiments. For KRas (d), from left to right, n = 1078, 1077, 952, 873, 954, 1039, 1059, and 1140 cells. For HRas (e), from left to right, n = 1158, 959, 1201, 950, 937, and 957 cells. For NRas (f), from left to right, n = 1449, 1422, 1138, 1203, 1131, 1472, 1393, and 1135 cells. All groups are significantly different from each other as assessed by one-way ANOVA, $p < 0.0001$ for both RasAR and RasAR(R89L) groups. Cohen's f values show effect sizes by one-way ANOVA and are indicated above each group. All violin plots show median and quartiles.

based on the activity of the co-expressed Ras. In cells expressing KRasS17N, biosensor fluorescence was distributed throughout the cytosol, whereas increased plasma membrane and perinuclear localization was observed upon co-expression with KRasG12C (Figure S2a). Colocalization analysis showed that the biosensor colocalizes with KRasG12C, but not KRasS17N (Figure S2a).

To examine whether RasAR detects the activities of Ras isoforms other than KRas, we assessed the functionality of RasAR in cells co-expressing RasAR and mCherry-tagged WT,

https://doi.org/10.1021/jacs.2c05203
J. Am. Chem. Soc. 2022, 144, 17432−17440

CA, or DN HRas and NRas in COS-7 cells. Similar to the results with KRas, co-expressing the biosensor with CA HRas or CA NRas led to enhanced colocalization between the biosensor and active Ras (Figure S2b,c) and significantly elevated C/Y emission ratios compared with the corresponding WT or DN variants (Figure 1e,f), independent of Ras overexpression levels (Figure S1d−f). The most pronounced difference in the C/Y emission ratio was observed between NRasS17N and NRasG13D populations, with a 66.9 ± 0.6 [mean ± SEM] % higher C/Y emission ratio ($\Delta R/R_0$) in the NRasG13D group, marking the dynamic range of the biosensor. Meanwhile, the R89L negative-control sensor displayed similar C/Y emission ratios regardless of the co-expressed Ras variant (Figure 1e,f). These data suggest that RasAR successfully reports on active Ras through changes in its C/Y emission ratio.

RasAR Captures Spatiotemporal Changes of Ras Activity in Living Cells. To determine whether RasAR can detect dynamic Ras activity, we co-expressed the sensor with mCherry-KRasWT in COS-7 cells and stimulated the cells with the epidermal growth factor (EGF). Upon activation of the Ras pathway, we observed a rapid increase in the C/Y emission ratio in cells expressing RasAR [Figure 2a; 17.0 ± 1.2% (mean ± s.e.m.), $t_{1/2}$ = 1.4 ± 0.15 min, n = 90 cells, 3 experimental replicates]. Consistent with previous studies,[26] we observed higher C/Y emission ratios in membrane ruffles following EGF stimulation, indicating enhanced KRas activity in these regions. In addition, consistent with the Golgi localization of Ras,[26] we observed an increased activity in the Golgi compartment (Figure 2a and Figure S4). Addition of EGFR inhibitor AG1478 then led to a decrease in the C/Y emission ratio (Figure 2a), showing the reversibility of RasAR. In contrast, cells co-expressing the RasAR (R89L) negative-control sensor with mCherry-KRasWT showed no emission ratio change.

In cells expressing mCherry-HRasWT or mCherry-NRasWT, EGF stimulation also led to increases in the RasAR C/Y emission ratio (Figure 2b,c; HRas: 21.0 ± 1.1%, $t_{1/2}$ = 1.11 ± 0.14 min; NRas: 14.1 ± 0.9%, $t_{1/2}$ = 1.5 ± 0.08 min; n = 90 cells from 3 experimental replicates, each), whereas no C/Y emission ratio increase was observed with the RasAR (R89L) negative control upon EGF stimulation. The EGF-stimulated increases in the emission ratio occurred in both the membrane ruffles as well as the Golgi compartment (Figure 2b,c and Figure S4), with slower kinetics observed at the Golgi (Figure S3a). Notably, NRasWT showed significantly slower activation kinetics than KRasWT and HRasWT (Supplementary Figure 3b).

To assess the ability of RasAR to detect changes in Ras activity in multiple cell types, we co-expressed RasAR with mCherry-HRasWT in HeLa and HEK293T cells. In both cell types, we observed an increase in the C/Y emission ratio, which was not observed in the negative-control sensor RasAR (R89L) (Figure S3d,e). We then compared the response of RasAR to the current Ras biosensor Ras-RAICHU-EV. EGF stimulation of COS-7 cells expressing Ras-RAICHU-EV led to a 13.5 ± 1.0% increase in a yellow-to-cyan emission ratio with a $t_{1/2}$ of 9.31 ± 0.28 min (Figure S3f,g, n = 65 cells from 3 experimental replicates), suggesting that the kinetics of Ras activity accumulation reported by Ras-RAICHU-EV were slower than those reported by RasAR. We then sought to validate RasAR responses with a pulldown assay measuring endogenous Ras activity. Notably, endogenous Ras showed fast

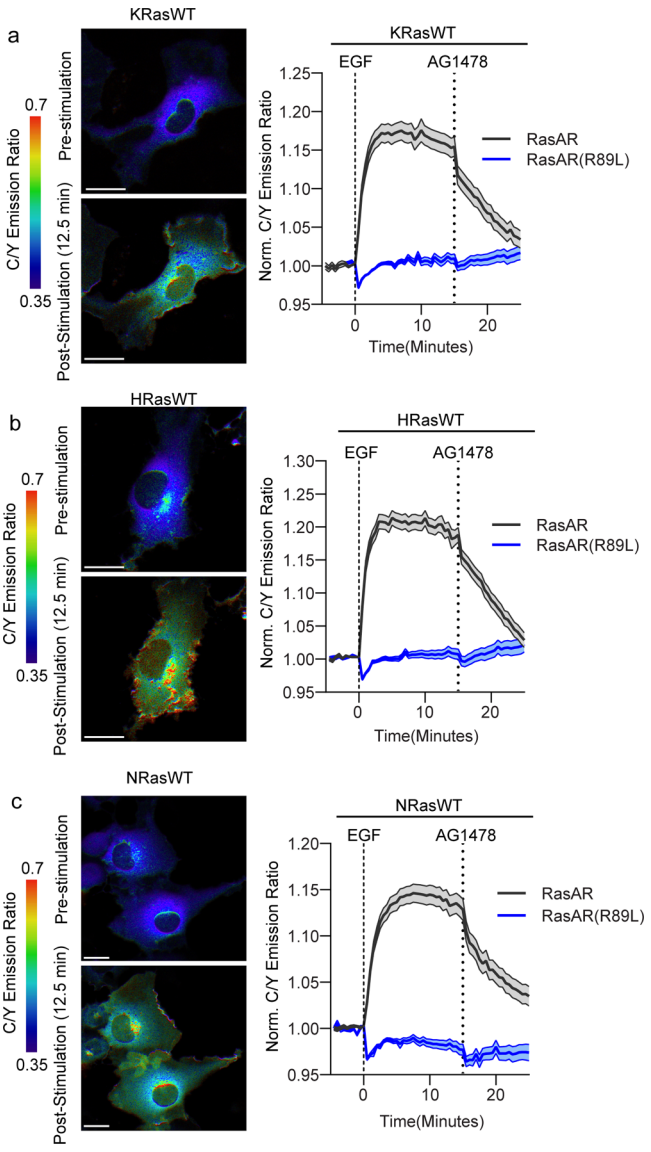

Figure 2. RasAR detects EGF-stimulated Ras activity in living cells. (a−c) Left, representative pseudocolor images of the C/Y emission ratios from COS-7 cells co-expressing RasAR along with mCherry tagged KRasWT, HRasWT, or NRasWT before (top) and 12.5 min after (bottom) EGF stimulation. Scale bars, 25 μm. Right, average time courses showing the C/Y emission ratio changes from RasAR (black curves) or the RasAR (R89L) negative-control mutant (blue curves) in cells co-expressing mCherry-RasWT and treated with 100 ng/mL EGF followed by 200 nM AG1478 as indicated. Combined results of three independent experiments, n = 90 cells per group. Solid lines indicate the mean, and shaded areas represent s.e.m.

kinetics reaching maximal activation within 5 min, similar to RasAR responses (Figure S3h). Together, these results suggest that RasAR is capable of reporting Ras activity dynamics in living cells.

RasAR Probes the Regulation of Ras by Src. Early reports using translocation probes indicated that HRas may be activated at the Golgi in response to EGF stimulation.[16,17] These initial studies proposed EGFR-mediated activation of Src as a prerequisite for Ras activity at the Golgi apparatus, as inhibition of Src with PP2 was shown to abrogate translocation of an RBD-GFP probe to the Golgi following EGF stimulation. However, other groups have shown an inhibitory role of Src via

https://doi.org/10.1021/jacs.2c05203
J. Am. Chem. Soc. 2022, 144, 17432−17440

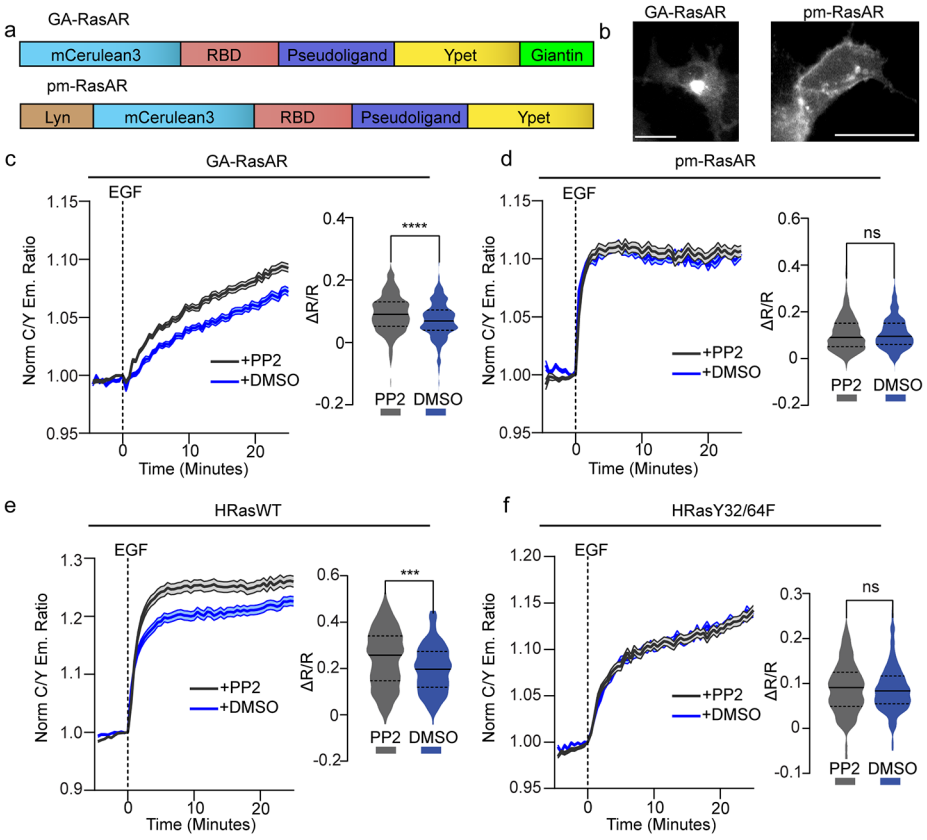

Figure 3. Probing Src regulation of HRas using RasAR. (a) Domain structures of GA-RasAR and pm-RasAR. (b) Representative images showing localization of targeted sensors. Scale bars, 25 μm. (c) Average time courses of the C/Y emission ratio change from GA-RasAR (left) and violin plots of the $\Delta R/R_0$ at t = 24 min (right) in COS-7 cells co-expressing mCherry-HRasWT and pretreated with the Src inhibitor PP2 (black, n = 300 cells) or DMSO control (blue, n = 300 cells). Mann−Whitney pairwise test, $p < 0.0001$. (d) Average time courses of the C/Y emission ratio change from pm-RasAR (left) and violin plots of the $\Delta R/R_0$ at t = 5.5 min (right) in COS-7 cells co-expressing mCherry-HRasWT and pretreated with the Src inhibitor PP2 (black, n = 300 cells) or DMSO control (blue, n = 300 cells). ns, not significant. (e) Average time courses of the C/Y emission ratio change from RasAR (left) and violin plots of the $\Delta R/R_0$ at t = 5.5 min (right) in COS-7 cells co-expressing mCherry- HRasWT and pretreated with the Src inhibitor PP2 (black, n = 180 cells) or DMSO control (blue, n = 180 cells). $p < 0.0001$. (f) Average time courses of the C/Y emission ratio change from RasAR (left) and violin plots of the $\Delta R/R_0$ at t = 5.5 min (right) in COS-7 cells co-expressing mCherry-HRasY32F/Y64F and pretreated with the Src inhibitor PP2 (black, n = 180 cells) or DMSO control (blue, n = 180 cells). n = 180 cells, $p < 0.0001$. Pooled results of 5 (c,d) or 3 (e,f) independent experiments. Solid lines in c−f indicate the mean, and shaded areas represent s.e.m. Violin plots in c−f display median and quartiles, and error bars represent s.e.m.

tyrosine phosphorylation at Y32 of HRas using a combination of pulldown assays and in vitro techniques, which preclude spatiotemporal analysis.[27] With its ratiometric readout and unimolecular design, RasAR is uniquely poised to measure cellular Ras activity within spatially defined compartments with the aid of subcellular targeting motifs. Noting this, we constructed two different RasAR variants, pm-RasAR, targeted to the plasma membrane with an N-terminal tag from Lyn kinase, and GA-RasAR, targeted to the Golgi apparatus via C-terminal fusion with a Giantin fragment (Figure 3a,b and Figure S5a,b). An increase in the C/Y emission ratio was observed in cells expressing GA-RasAR and mCherry-HRasWT stimulated with EGF but not in cells expressing a negative-control sensor, GA-RasAR (R89L) (Figure S5c). Similarly, pm-RasAR showed an EGF-stimulated increase in C/Y emission when co-expressed with mCherry-HRasWT in COS-7 cells, which was not observed in cells treated with vehicle control (Figure S5d). EGF-induced Ras activity increases showed distinct kinetics at the plasma membrane and Golgi compartment, with a longer $t_{1/2}$ for GA-RasAR compared to pm-RasAR (Figure S5e, $t_{1/2}$ = 5.3 ± 0.4 min for GA-RasAR, $t_{1/2}$ = 0.86 ± 0.07 min for pm-RasAR, $p < 0.0001$), consistent with the trend observed using cytosolic RasAR (Figure S3a). These results corroborate previous studies showing delayed and prolonged HRas activation at the Golgi apparatus in response to EGF stimulation.[16]

To clarify the regulatory role of Src on HRas at the Golgi, we monitored HRas activity at the Golgi with GA-RasAR in the presence of Src inhibitor PP2. As shown in Figure 3c, in cells expressing GA-RasAR and mCherry-HRas, EGF-induced responses were enhanced by PP2 pretreatment (n = 300 cells each for PP2 and DMSO-treated groups, $p < 0.0001$), suggesting an inhibitory role for Src on Ras activity at the Golgi. Interestingly, PP2 pretreatment did not affect EGF-induced Ras activity at the plasma membrane (Figure 3d). In sum, these results suggest that Src inhibition increases EGF-induced Ras activity specifically in the Golgi compartment, but not at the plasma membrane.

Cytosolic RasAR, when co-expressed with HRasWT, showed a larger EGF-induced response with PP2 pretreatment (Figure 3e, n = 180 cells, $p < 0.001$). Additionally, treatment with the more specific Src inhibitor SrcI1 similarly enhanced EGF-

https://doi.org/10.1021/jacs.2c05203
J. Am. Chem. Soc. 2022, 144, 17432−17440

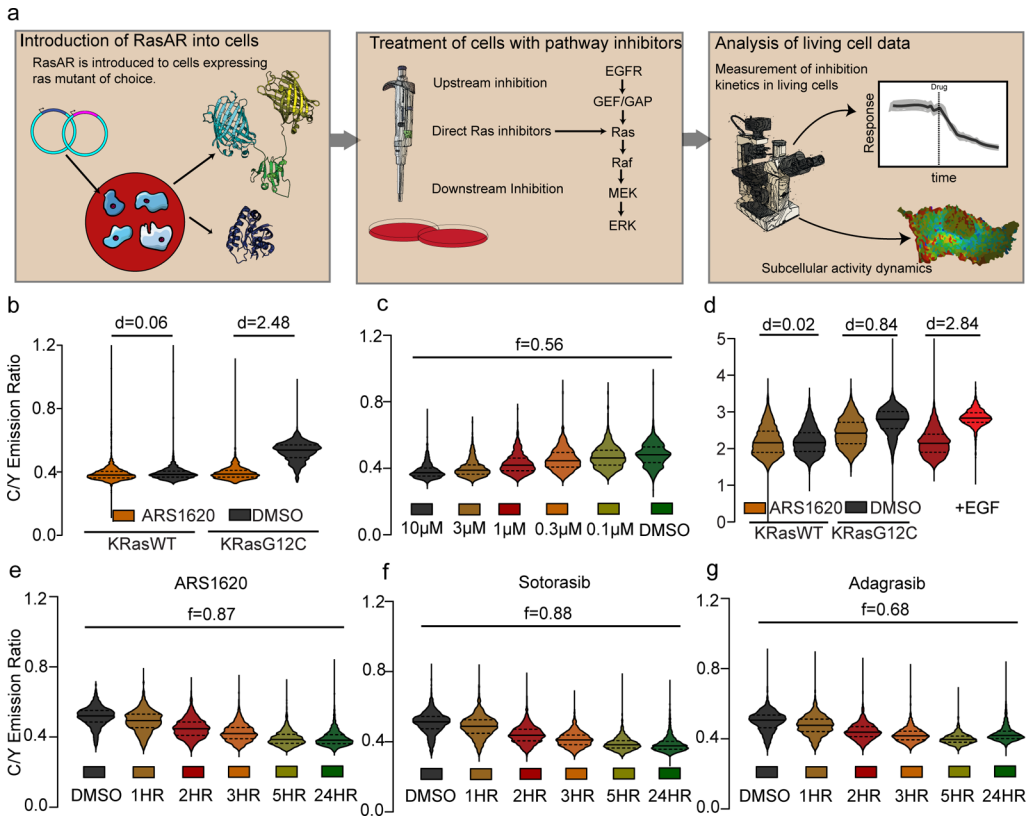

Figure 4. RasAR measures Ras inhibition in living cells. (a) General schematic of our Ras inhibition assay. RasAR is introduced to cells expressing mutant Ras and treated with Ras pathway inhibitors. Spatiotemporal differences in the activity of Ras as well as the entire signaling pathway caused by inhibitor treatment can be visualized in living cells to provide information about target engagement. Fluorescent protein and Ras structures (PDB 4G0N, 1YFP, 4KW4) are used in the schematic. (b) C/Y emission ratios of COS-7 cells co-expressing mCherry-KRasG12C or KRasWT plus RasAR treated with either ARS1620 (10 μM) or DMSO for 24 h. (c) C/Y emission ratios of COS-7 cells co-expressing mCherry-KRasG12C and RasAR-treated with the indicated concentrations of ARS1620 for 24 h. (d) Y/C emission ratios of COS-7 cells co-expressed mCherry-KRasG12C and EKAR treated with ARS1620 (10 μM) for 3 h. EGF control included to verify EKAR response. (e–g) C/Y emission ratios recorded from COS-7 cells co-expressing RasAR and mCherry-KRasG12C after incubation with (e) ARS1620 (10 μM), (f) Sotorasib (10 μM), or (g) Adagrasib (10 μM) for the indicated times. Each data set is pooled from three independent experiments. For (b), from left to right, n = 1082, 1116, 1038, and 1153 cells. For (c), from left to right, n = 1156, 1037, 1076, 1029, 962, and 866 cells. For (d), from left to right, n = 4668, 3902, 4056, 3162, 2033, and 2454 cells. For (e), from left to right, n = 2170, 2094, 2226, 2172, 2203, and 2833 cells. For (f), from left to right, n = 2447, 2610, 2398, 2777, 2851, and 4287 cells. For (g), from left to right, n = 1932, 2055, 1986, 1770, 1952, and 2161 cells. Violin plots show median and quartiles. Cohen's d-statistic from pairwise t-test displayed for (b) and (d). For (c) and (e–f), one-way ANOVA is performed with Cohen's f-statistic displayed. All groups significantly different from each other by one-way ANOVA (c,e–h), or by t-test (b,d), $p < 0.0001$.

induced Ras activity (Figure S5f, n = 150 cells for SrcI1, n = 144 for DMSO, $p < 0.0001$). Phosphorylation of residue Y32 has been implicated in the negative regulation of HRas by Src.[27] To verify this mechanism of Src inhibition, we co-expressed RasAR with HRasY32F and stimulated with EGF. However, mutating Y32 did not abolish the inhibitory effect of Src on HRas, as PP2-pretreated cells still showed an enhanced response to EGF in comparison with control cells (Figure S5g). KRas was recently shown to be negatively regulated by Src via dual phosphorylation of Y32 and Y64,[28] which negatively impacts multiple steps of the GTPase cycle and impairs binding to effectors. However, the role of Y64 in HRas has not been investigated. To test the hypothesis that phosphorylation of both Y32 and Y64 is involved in Src regulation of HRas, we expressed RasAR and an mCherry-labeled HRas mutant containing Y32F/Y64F mutations and monitored EGF-induced responses in the presence and absence of PP2. In this case, we observed no significant difference between PP2-pretreated cells and control cells (Figure 3f, n = 180 cells each for PP2- and DMSO-treated groups). These data indicate that Src plays an inhibitory role in EGF-induced HRas activity in a manner that specifically targets subcellular pools of Golgi Ras and involves Y64.

RasAR Detects Ras Inhibition in Living Cells. Ras is a prominent oncogene and an extensively pursued molecular target for cancer therapy. However, cellular assays for characterizing inhibitor effects require the use of Ras pulldown assays, which are cumbersome and difficult to extend to high throughput. Furthermore, these assays require cell lysis and do not allow for characterization of spatiotemporal activities of the inhibitors. With a ratiometric biosensor capable of measuring Ras activity, we sought to measure live-cell Ras inhibition with RasAR. This assay should allow for quantitative measurement of Ras inhibition in living cells with high spatiotemporal resolution. Temporal dynamics of Ras inhibition can be tracked and subcellular inhibitory effects can be compared to provide important information about target engagement in living cells (Figure 4a). In addition, the intact cellular environment contains the entire Ras/Raf/extracellular signal-regulated kinase (ERK) signaling pathway[29] and additional cross-regulatory networks, which should allow for testing of inhibitory effects on the entire pathway.

https://doi.org/10.1021/jacs.2c05203
J. Am. Chem. Soc. 2022, 144, 17432–17440

To test the utility of RasAR in a live-cell Ras inhibitor assay, we first focused on ARS1620, a previously developed KRasG12C inhibitor, which binds to GDP-bound KRasG12C and prevents nucleotide exchange.[10] Cells co-expressing KRasG12C and RasAR were incubated with 10 μM ARS1620 or DMSO for 24 h. We observed a higher C/Y emission ratio in KRasG12C-expressing cells treated with DMSO compared with ARS1620 treatment, whereas KRasWT controls showed no effect of inhibitor treatment (Figure 4b). Additionally, we tested different concentrations (10, 3, 1, 0.3, and 0.1 μM) of ARS1620 in COS-7 cells expressing both RasAR and mCherry-KRasG12C. Decreasing dosages of ARS1620 corresponded to higher C/Y emission ratios, demonstrating the capability of RasAR to measure dose-dependent inhibition of KRasG12C in living cells (Figure 4c). Assessing Ras expression by RFP intensity suggested that differences in the C/Y emission ratio are related to changes in activity and not expression levels (Figure S6a,b). To further demonstrate the capability of live-cell assays for characterizing Ras inhibitors, we next sought to test the effect of ARS1620 on the Ras signaling pathway by using our ERK activity reporter (EKAR4)[30] to measure the activity of the key downstream master regulator ERK. EKAR4 serves a surrogate substrate of ERK and reports ERK-mediated phosphorylation as an increase in FRET between CFP and YFP. We co-expressed mCherry-KRasG12C with EKAR4 and treated the cells with ARS1620 (Figure 4d). As expected, we observed a larger effect of ARS1620 treatment on the EKAR4 Y/C emission ratio in mCherry-KRasG12C expressing cells, compared to mCherry-KRasWT expressing COS-7 cells (Figure 4d, Cohen's d = 0.02, 0.84 for KRasWT and KRasG12C, respectively), indicating that ARS1620 can effectively inhibit the Ras−ERK pathway in KRasG12C expressing cells.

We next assessed the kinetics of KRasG12C inhibition by treating RasAR and KRasG12C co-expressing COS-7 cells with 10 μM ARS1620 and measuring the C/Y emission ratio at different time points (Figure 4e). Surprisingly, we observed a steady decline in the C/Y emission ratio over the first 5 h of treatment (Table S1), suggesting relatively slow cellular kinetics, which may correspond to the slow intrinsic rate of GTP hydrolysis by KRasG12C. Given that KRasG12C is continually being synthesized during these experiments, we next tested whether ongoing protein synthesis contributes to the slow inhibition kinetics that we observed by treating cells with ARS1620 in the presence of cycloheximide. As expected, cycloheximide treatment reduced KRasG12C expression levels, confirming that KrasG12C is re-synthesized within the 24-h timeframe of our assay (Figure S6c). However, inhibiting this re-synthesis did not speed up the kinetics of Ras inactivation (Figure S6d and Table S1). We also considered the possibility that the slow kinetics of inhibition were related to Ras overexpression; however, dividing cells into low-, medium-, and high-expression groups according to RFP intensity revealed no relationship between the kinetics of inhibition and KRasG12C expression levels (Figure S6e−h). To further investigate Ras inhibition kinetics, we treated cells with Sotorasib[12] or Adagrasib,[31] two additional KRasG12C inhibitors. We observed s imilar inhibition kinetics with Sotorasib and Adagrasib, with a continuous C/Y emission ratio decrease for the first 5 h post treatment (Figure 4f−g and Table S1). In addition, the slow inhibition kinetics of Sotorasib was also observed at the ERK activity level shown by EKAR4 emission ratio changes (Figure S6i). These data demonstrate the utility of RasAR in the context of Ras inhibition assays, making it possible to bring live-cell data to the field of Ras inhibitor development.

DISCUSSION

We developed a new biosensor, RasAR, featuring a pseudoligand-based design, to report dynamic changes in compartment-specific Ras activities in living cells. Compared with traditional biochemical assays, RasAR enables live-cell tracking of Ras activity dynamics. RasAR provides a ratiometric readout, allowing for the cancellation of cellular variations and quantitative measurement of Ras activity. Compared with current Ras biosensors, the Ras Raichuseries, the main advantage of RasAR is that the biosensor itself does not contain Ras and is therefore capable of measuring cellular activity of different Ras isoforms. We demonstrated the fast kinetics of RasAR, which correlate well with endogenous Ras activation, whereas Ras-RAICHU-EV showed slow kinetics, possibly due to steric hindrance of the embedded Ras within the unimolecular construct. Furthermore, RasAR allows for interrogation of subcellular Ras activity in living cells via a genetic targeting approach.[14,32] The dynamic range of RasAR (66.9 ± 0.6%) is on par or even compares favorably with many widely used FRET-based biosensors.[30,33,34] While RasAR is currently capable of detecting the activity of co-expressed Ras in COS-7 cells, it does not show clear responses to EGF stimulation in COS-7 cells with only endogenous Ras expression. Ongoing experiments will test its capability of detecting endogenous Ras activity in a variety of cancer cell lines. Future development will also focus on further enhancing the sensitivity and dynamic range of RasAR to sensitively measure endogenous Ras activity. In particular, we hypothesize that enhancing the affinity of the RBD toward active Ras will be critical for detecting endogenous Ras activity, as previous research has demonstrated that wildtype RBD has insufficient affinity to effectively outcompete endogenous Ras effectors within the cell.[35]

It was unclear whether the different Ras isoforms follow similar activation kinetics. From our findings, NRas has the slowest kinetics among the Ras isoforms, a property that may be related to the unique subcellular localization of this isoform.[36] NRas has a distinct hypervariable region, with post-translational modifications consisting of a single cysteine palmitoylation in addition to the C-terminal cysteine farnesylation, which is conserved among all Ras isoforms. This differs from the dual palmitoylation of HRas, and the polybasic stretch of KRas.[4,37] While HRas and KRas both show prominent localization at the plasma membrane, with some Golgi localization,[26] consistent with the activity detected at these locations by RasAR (Figure 2a,b and Figure S4), a substantial portion of NRas has also been observed to accumulate at the Golgi apparatus and in the cytoplasm, where it forms a complex with VPS35.[36] The unique post-translational modifications and distinct cellular distribution of NRas may contribute to its delayed activation, as EGF-stimulated rapid Ras activation is mediated by Sos-induced nucleotide exchange at the plasma membrane. Given that cytosolic NRas is protected by the carrier VPS35, this pool of NRas may not exhibit significant activity. Indeed, the majority of NRas activity that we detected with RasAR occurred at the plasma membrane and Golgi (Figure 2c and Figure S4).

RasAR also revealed the nature of Src regulation of Ras activity at the Golgi compartment. In stark contrast to a

https://doi.org/10.1021/jacs.2c05203
J. Am. Chem. Soc. 2022, 144, 17432−17440

previous model in which Src promotes Golgi Ras activity, we showed that Src negatively regulates Ras activity at the Golgi compartment, but not at the plasma membrane (Figure 3). This discrepancy may result from the use of different cell systems. For example, RasGRP1, a Ras GEF that has been suggested to act downstream of Src, is endogenously expressed in PC12 cells, but not in COS-7 cells.[38] Mechanistically, our data suggest that Src regulates Golgi HRas through phosphorylation of tyrosines 32 and 64, contrasting with previous studies[27] and identifying Y64 as an important mechanistic link in Src regulation of HRas. Residue Y64 is conserved among Ras isoforms. Thus, similar to previous reports with KRas[28] and our results with HRas, Y64 likely plays a critical role in NRas function as well. How does Src achieve specific regulation of the Golgi pool of HRas? Further experiments will explore subcellular differences in Src activity.[39] Interestingly, it has been demonstrated that Ras signaling at the Golgi compartment acts through Ral GTPase, antagonizes ERK activity, and promotes apoptosis in MCF-7 cells.[40] On the other hand, it was shown that site-selective activation of Ras at the Golgi can produce Golgi-specific ERK activation.[41] Future experiments will examine the downstream effects of Src regulation on the Ras pathway. The specific subcellular regulation identified here thus adds to an already very complex picture of subcellular Ras activity that is differentially regulated and coupled to downstream signaling.

While development of effective inhibitors to target oncogenic Ras mutants is an ongoing pursuit, RasAR offers an amenable strategy for fluorescence imaging of Ras activity dynamics in living cells treated with different candidate inhibitors. KRasG12C inhibitors such as ARS1620 and Sotorasib bind to the Switch II pocket found in GDP-bound KRasG12C. The binding of these inhibitors prevents Sos-induced nucleotide exchange and abrogates signaling activity.[8,10] Using a RasAR-based live-cell assay, we found that the maximal effect of these KRasG12C inhibitors requires at least 5 h, longer than the 2-h window for achieving full target engagement suggested by previous mass spectrometry experiments,[10] yet similar to previous studies of ARS853 utilizing Ras pulldown assays.[8] One explanation for this discrepancy may lie within the details of the assays and models employed. In previous studies, cells were lysed prior to engagement or activity measurements in mouse or cell models expressing endogenous KRasG12C. In contrast, our data were collected in living cells where KRasG12C was co-expressed with our fluorescent biosensor. It is possible that different expression levels of KRasG12C play a role in producing different results, although we did not observe a dependence of the inhibitory effect on the expression levels of KRasG12C in different cells (Figure S6e−h). In fact, the slow kinetics that we observed are consistent with the idea that KRasG12C inhibition by these compounds requires nucleotide cycling and cooperation from cellular factors. GDP-bound KRasG12C can be formed via intrinsic GTPase activity or specific GAPs but can also be removed by cellular GEFs. The kinetics of KRas inhibition are therefore intrinsically slower than for inhibition of a single target, as previously shown in the case of ARS853.[8] Considering the role that GEFs and GAPs play in regulating the nucleotide state of KRasG12C mutants, cell-type specific differences in these regulators may also affect inhibition kinetics. The ability to detect this residual Ras activity showcases the sensitivity of our live-cell Ras inhibition assay, which can be used to investigate the influence of other cellular factors, test combination therapies, and explore potential resistance mechanisms. RasAR is therefore a powerful tool not only for probing isoform-selective and location-specific Ras signaling but also for revealing live-cell properties and behaviors of Ras inhibitors.

METHODS

Gene Construction. All constructs were generated using a one-step multi-fragment Gibson Assembly reaction (NEB 2× High Fidelity Master Mix). All fragments were PCR-amplified with Q5 polymerase (NEB). For RasAR, mCerulean3 was generated via PCR amplification using primers 1 and 2 (see Table S2). The RBD with 3′-pseudoligand was amplified using overlap extension from CRY2PHP-mCherry-Raf1, a gift from the Cui Lab,[42] using primers 3 and 4. YPet with a 3′-NES (LPPLERLTL) was amplified using primers 5 and 6. pcDNA3.1+ (Invitrogen) backbone, incorporating the NES overlap sequence, was synthesized in two fragments by Gibson assembly with primer pairs 7/8. For GA-RasAR, RasAR without any targeting motif was amplified using primers 9 and 10. pcDNA3.1+ with a 5′ Giantin tag and 8-residue linker was amplified from CIAR-Golgi, provided by the Maly lab,[43] using primers 11 and 12. For pm-RasAR, the N-terminal Lyn-targeting motif was amplified with overlap extension using primers 13 and 14. Untargeted RasAR was amplified with primers 15 and 16. Ras constructs are gifts from Maly, Inoue, and Devaraj labs, with mCherry tagged at the N-terminal. Codon-optimized KRasWT and NRasWT with overlap sequences, 5′-AAGCTGGCTAGCGTTTAAACTTAAGCTTGCCACC- and -TCTAGAGGGCCCGTTTAAACCCGCTGATCAGC-3′, were purchased from Genscript. These constructs were amplified with primers 31 and 32. The fidelity of construct assembly was verified by Sanger sequencing.

Cell Culture. COS-7 cells were cultured in Dulbecco modified Eagle medium (DMEM, Gibco) containing 4.5 g/L glucose and supplemented with 10% (v/v) fetal bovine serum (FBS; Sigma) and 1% (v/v) penicillin−streptomycin (Pen-Strep, Sigma-Aldrich). Cells were maintained in a humidity-controlled incubator at 37 °C with 5% CO_2. Cells were seeded onto sterile 35-mm glass-bottomed dishes and grown to 50−70% confluency. Cells were transfected with PolyJet (SignaGen Laboratories) 24 h prior to imaging. Prior to transfection, the COS-7 cells were washed with Dulbecco phosphate-buffered saline (DPBS, Gibco), and medium was changed to a serum-free DMEM to serum-starve the cells for 24 h during transfection prior to imaging.

Ras-GTP Pulldown Assay. COS-7 cells were starved in serum-free medium for 24 h, stimulated with 100 ng/mL EGF, and then collected at different time points following stimulation. Cells ($2-3 \times 10^6$ cells) were rinsed with ice-cold PBS and then lysed with 300 μL of lysis/binding/wash buffer (25 mM Tris−HCl, pH 7.2, 150 mM NaCl, 5 mM $MgCl_2$, 5% glycerol, 1% NP40) from Active Ras Detection kit (Cell Signaling Technology, #8821) supplemented with complete, EDTA-free protease cocktail inhibitors (Millipore Sigma, 11697498001), 1 mM PMSF, and 80 μg of GST-Raf-RBD (Cell signaling Technology, #8821). Lysates were votexed briefly, incubated on ice for 5 min, and subsequently pre-cleared at 16,000×g at 4 °C for 15 min. 90% of the pre-cleared lysates were subsequently added to prewashed glutathione agarose beads from Active Ras Detection kit (Cell signaling Technology, #8821) for 1 h at 4 °C under constant rocking. 5−10% of the lysates were saved for total Ras analysis. The beads were then spun down and washed once with lysis/binding/wash buffer and eluted with 50 μL of 2× SDS-PAGE sample buffer with 200 mM dithiothreitol. The eluted samples were heated for 5 min at 98 °C and used for Western blotting to determine the level of GTP-bound Ras. Protein was separated via 4−15% SDS-PAGE and transferred to PVDF membranes. The membranes were blocked with TBS containing 0.1% Tween-20 and 5% bovine serum albumin and then incubated with rabbit anti-Ras antibody (CST, #3965, 1:1000) overnight at 4 °C. After incubation with the goat anti-Rabbit horseradish peroxidase-conjugated secondary antibody, the membranes were developed using horseradish peroxidase-based chem-

https://doi.org/10.1021/jacs.2c05203
J. Am. Chem. Soc. 2022, 144, 17432−17440

iluminescent substrates (34,579 and 34,076, Thermoscientific). The intensity of the bands was quantified with ImageJ 1.52 s software. Active GTP-bound Ras was normalized to total Ras in cell lysate.

Time-Lapse Widefield Epifluorescence Imaging. Cells were washed three times with Hanks's balanced salt solution (HBSS, Gibco) prior to imaging. Cells were imaged in HBSS in the dark at 37 °C. The EGF (Sigma-Aldrich), AG1478 (Selleckchem, S2728), MRTX-1257 (MedChemExpress, HY-114436), Sotorasib (MedChemExpress, HY-114277), and ARS1620 (gift of Kevan Shokat, University of California San Francisco) were added at the indicated concentrations. Cells were imaged on a Zeiss Axio Observer Z1 microscope equipped with a 20×/0.8 NA objective and a Hamamatsu Flash 4.0 sCMOS camera, controlled using MicroManager 2.0 software. For time series, images from multiple fields of view were acquired at each time point at 30 s intervals. RFP was imaged using a 568DF55 excitation filter, a 600DRLP dichroic mirror, and a 653DF95 emission filter. CFP was imaged using a 420DF20 excitation filter, a 455DRLP dichroic mirror, and a 470DF40 emission filter. CYFRET was imaged using a 420DF20 excitation filter, a 455DRLP dichroic mirror, and a 535DF25 emission filter. YFP was imaged using a 495DF10 excitation filter, a 515DRLP dichroic mirror, and a 535DF25 emission filter. Exposure times for each channel were 250−500 ms. All filter sets were controlled by a Lambda 10−2 filter-changer (Sutter Instruments). All fluorescence images were background-corrected by rolling circle background subtraction in ImageJ using a rolling-ball circle radius of 350 pixels. Cyan/yellow or yellow/cyan emission ratios were then calculated by dividing the CFP channel values by the CYFRET channel values or the CYFRET channel values by CFP channel values, respectively. For the time-series analysis, all values were normalized to the time point prior to drug addition by dividing each value by the basal ratio value prior to drug addition. Co-expression experiments were processed using Cell Profiler on background-subtracted images and segmented using CYFRET channel images. Individual $t_{1/2}$ measurements were acquired using custom script within MATLAB.

Statistics and Reproducibility. All imaging experiments were performed with independent experimental replicates with all replicate attempts being successful. Experiments from Figures 1, 2, 3e−f, 4, S1, S3, and S5f−g were performed with three independent replicates. Five independent replicates were performed for Figure 3c−d. Two experimental replicates were performed, as shown in Figures S5c,d,g and S6. Statistical analyses were performed using GraphPad Prism 8 (GraphPad Software). In data sets with large sample sizes (Figures 1, 4, and S6), small effects led to statistically significant changes in typical statistical comparisons. Due to this, we performed Cohen's *f*, effect size calculations based on one-way ANOVA, and Cohen's d, effect size calculations based on pairwise t-test. For smaller data sets (Figures 3, S2, S3, and S5), Mann−Whitney pairwise comparisons are performed. Averaged live-cell imaging time courses depict mean ± S.E.M.; violin plots depict the median and quartiles, as indicated in the figure legends.

■ ASSOCIATED CONTENT

Supporting Information

The Supporting Information is available free of charge at https://pubs.acs.org/doi/10.1021/jacs.2c05203.

Additional experiments performed to support the results of the main figures of the text including colocalization analyses, relative expression level analyses, and western blot (PDF)

■ AUTHOR INFORMATION

Corresponding Author

Jin Zhang − *Department of Pharmacology, Department of Chemistry and Biochemistry, and Department of Bioengineering, University of California, San Diego, La Jolla, California 92093, United States;* orcid.org/0000-0001-7145-7823; Phone: (858) 246-0602; Email: jzhang32@ucsd.edu

Authors

Ryan Weeks − *Department of Pharmacology and Department of Chemistry and Biochemistry, University of California, San Diego, La Jolla, California 92093, United States*

Xin Zhou − *Department of Pharmacology, University of California, San Diego, La Jolla, California 92093, United States;* orcid.org/0000-0003-0734-0828

Tina L. Yuan − *Novartis Institutes for Biomedical Research, Cambridge, Massachusetts 02139, United States*

Complete contact information is available at: https://pubs.acs.org/10.1021/jacs.2c05203

Notes

The authors declare no competing financial interest.

All data supporting the findings of this study are available upon reasonable request.

Custom ImageJ macros and MATLAB code used to analyze imaging data are available upon reasonable request.

■ ACKNOWLEDGMENTS

We thank Drs. Bianxiao Cui, Takanari Inoue, Neal Devaraj, and Dustin Maly for providing various constructs, Dr. Kevan Shokat for providing ARS1620, Dr. Christopher Booth for initial cloning and testing of candidate constructs, Dr. Yang An for helpful discussions about statistics, and Dr. Sohum Mehta for critical reading of the manuscript and help with graphic designs. This work was supported by NIH grant R35 CA197622 and Novartis Institutes for BioMedical Research (NIBR) Global Scholar program (J.Z.) as well as NIH NS047101 to the UCSD Microscopy Core.

■ REFERENCES

(1) Lowy, D. R.; Willumsen, B. M. Function and Regulation of Ras. *Annu. Rev. Biochem.* **1993**, *62*, 851−891.

(2) Lu, S.; et al. Ras Conformational Ensembles, Allostery, and Signaling. *Chem. Rev.* **2016**, *116*, 6607−6665.

(3) Terrell, E. M.; Morrison, D. K. Ras-mediated activation of the Raf family kinases. *Cold Spring Harbor Perspect. Med.* **2019**, *9*, No. a033746.

(4) Mo, S. P.; Coulson, J. M.; Prior, I. A. RAS variant signalling. *Biochem. Soc. Trans.* **2018**, *46*, 1325−1332.

(5) Prior, I. A.; Hancock, J. F. Ras trafficking, localization and compartmentalized signalling. *Semin. Cell Dev. Biol.* **2012**, *23*, 145−153.

(6) Simanshu, D. K.; Nissley, D. V.; McCormick, F. RAS Proteins and Their Regulators in Human Disease. *Cell* **2017**, *170*, 17−33.

(7) Stalnecker, C. A.; Der, C. J. RAS, wanted dead or alive: Advances in targeting RAS mutant cancers. *Sci. Signaling* **2020**, *13*, No. eaay6013.

(8) Lito, P.; Solomon, M.; Li, L. S.; Hansen, R.; Rosen, N. Cancer therapeutics: Allele-specific inhibitors inactivate mutant KRAS G12C by a trapping mechanism. *Science* **2016**, *351*, 604−608.

(9) Patricelli, M. P.; et al. Selective inhibition of oncogenic KRAS output with small molecules targeting the inactive state. *Cancer Discovery* **2016**, *6*, 316−329.

(10) Janes, M. R.; et al. Targeting KRAS Mutant Cancers with a Covalent G12C-Specific Inhibitor. *Cell* **2018**, *172*, 578−589.e17.

(11) Ostrem, J. M.; Peters, U.; Sos, M. L.; Wells, J. A.; Shokat, K. M. RASG (12C) inhibitors allosterically control GTP affinity and effector interactions Supplementary Information. *Nature* **2013**, *503*, 1−551.

(12) Blair, H. A. Sotorasib: First Approval. *Drugs* **2021**, *81*, 1573.

(13) Baker, M. J.; Rubio, I. Active GTPase Pulldown Protocol. *Methods Mol. Biol.* **2021**, *2262*, 117−135.
(14) Lang, P.; Yeow, K.; Nichols, A.; Scheer, A. Cellular imaging in drug discovery. *Nat. Rev. Drug Discovery* **2006**, *5*, 343−356.
(15) Bivona, T. G.; Quatela, S.; Philips, M. R. Analysis of Ras Activation in Living Cells with GFP-RBD. *Methods Enzymol.* **2006**, *407*, 128−143.
(16) Chiu, V. K.; et al. Ras signalling on the endoplasmic reticulum and the Golgi. *Nat. Cell Biol.* **2002**, *4*, 343−350.
(17) Bivona, T. G.; et al. Phospholipase Cγ activates Ras on the Golgi apparatus by means of RasGRP1. *Nature* **2003**, *424*, 694−698.
(18) Rubio, I.; et al. TCR-Induced Activation of Ras Proceeds at the Plasma Membrane and Requires Palmitoylation of N-Ras. *J. Immunol.* **2010**, *185*, 3536−3543.
(19) Augsten, M.; et al. Live-cell imaging of endogenous Ras-GTP illustrates predominant Ras activation at the plasma membrane. *EMBO Rep.* **2006**, *7*, 46−51.
(20) Mochizuki, N.; et al. Spatio-temporal images of growth-factor-induced activation of Ras and Rap1. *Nature* **2001**, *411*, 1065−1068.
(21) Bery, N.; et al. BRET-based RAS biosensors that show a novel small molecule is an inhibitor of RAS-effector protein-protein interactions. *Elife* **2018**, *7*, 1−28.
(22) Greenwald, E. C.; Mehta, S.; Zhang, J. Genetically encoded fluorescent biosensors illuminate the spatiotemporal regulation of signaling networks. *Chem. Rev.* **2018**, *118*, 11707−11794.
(23) Fetics, S. K.; et al. Allosteric effects of the oncogenic rasq61l mutant on raf-RBD. *Structure* **2015**, *23*, 505−516.
(24) Ohnishi, M.; et al. Selective inhibition of Ras interaction with its particular effector by synthetic peptides corresponding to the Ras effector region. *J. Biol. Chem.* **1998**, *273*, 10210−10215.
(25) Kiel, C.; Serrano, L.; Herrmann, C. A detailed thermodynamic analysis of Ras/effector complex interfaces. *J. Mol. Biol.* **2004**, *340*, 1039−1058.
(26) Choy, E.; et al. Endomembrane trafficking of ras: The CAAX motif targets proteins to the ER and Golgi. *Cell* **1999**, *98*, 69−80.
(27) Bunda, S.; et al. Src promotes GTPase activity of Ras via tyrosine 32 phosphorylation. *Proc. Natl. Acad. Sci. U. S. A.* **2014**, *111*, E3785−E3794.
(28) Kano, Y.; et al. Tyrosyl phosphorylation of KRAS stalls GTPase cycle via alteration of switch I and II conformation. *Nat. Commun.* **2019**, *10*, 224.
(29) Lavoie, H.; Gagnon, J.; Therrien, M. ERK signalling: a master regulator of cell behaviour, life and fate. *Nat. Rev. Mol. Cell Biol.* **2020**, *21*, 607−632.
(30) Keyes, J.; et al. Signaling diversity enabled by rap1-regulated plasma membrane ERK with distinct temporal dynamics. *Elife* **2020**, *9*, 1−18.
(31) Hallin, J.; et al. The KRASG12C inhibitor MRTX849 provides insight toward therapeutic susceptibility of KRAS-mutant cancers in mouse models and patients. *Cancer Discovery* **2020**, *10*, 54−71.
(32) Zhou, X.; Mehta, S.; Zhang, J. Genetically Encodable Fluorescent and Bioluminescent Biosensors Light Up Signaling Networks. *Trends Biochem. Sci.* **2020**, *45*, 889−905.
(33) Allen, M. D.; Zhang, J. Subcellular dynamics of protein kinase A activity visualized by FRET-based reporters. *Biochem. Biophys. Res. Commun.* **2006**, *348*, 716−721.
(34) Zhou, X.; et al. Dynamic Visualization of mTORC1 Activity in Living Cells. *Cell Rep.* **2015**, *10*, 1767−1777.
(35) Wiechmann, S.; et al. Conformation-specific inhibitors of activated Ras GTPases reveal limited Ras dependency of patient-derived cancer organoids. *J. Biol. Chem.* **2020**, *295*, 4526−4540.
(36) Zhou, M.; et al. VPS35 binds farnesylated N-Ras in the cytosol to regulate N-Ras trafficking. *J. Cell Biol.* **2016**, *214*, 445−458.
(37) Zhou, B.; Der, C. J.; Cox, A. D. The role of wild type RAS isoforms in cancer. *Semin. Cell Dev. Biol.* **2016**, *58*, 60−69.
(38) Rubio, I.; et al. Ras activation in response to phorbol ester proceeds independently of the EGFR via an unconventional nucleotide-exchange factor system in COS-7 cells. *Biochem. J.* **2006**, *398*, 243−256.
(39) Seong, J.; et al. Visualization of Src Activity at Different Compartments of the Plasma Membrane by FRET Imaging. *Chem. Biol.* **2009**, *16*, 48−57.
(40) Casar, B.; et al. RAS at the Golgi antagonizes malignant transformation through PTPRκ-mediated inhibition of ERK activation. *Nat. Commun.* **2018**, *9*, 3595.
(41) Komatsu, T.; et al. Organelle-specific, rapid induction of molecular activities and membrane tethering. *Nat. Methods* **2010**, *7*, 206−208.
(42) Zhang, K.; et al. Light-mediated kinetic control reveals the temporal effect of the Raf/MEK/ERK pathway in PC12 cell neurite outgrowth. *PLoS One* **2014**, *9*, No. e92917.
(43) Rose, J. C.; et al. A computationally engineered RAS rheostat reveals RAS-ERK signaling dynamics. *Nat. Chem. Biol.* **2017**, *13*, 119−126.

Recommended by ACS

Fluorescence Anisotropy Assay with Guanine Nucleotides Provides Access to Functional Analysis of Gαi1 Proteins
Anna Pepanian, Markus Pietsch, *et al.*
OCTOBER 07, 2022
ANALYTICAL CHEMISTRY
READ

Covalent Solvatochromic Proteome Stress Sensor Based on the Schiff Base Reaction
Di Shen, Yu Liu, *et al.*
OCTOBER 04, 2022
ANALYTICAL CHEMISTRY
READ

Site-Specific ^{19}F NMR Method for Detecting Arf6 GEF Activity
Jiarong Wang, Junfeng Wang, *et al.*
JUNE 06, 2022
ANALYTICAL CHEMISTRY
READ

Construction of a Mass-Tagged Oligo Probe Set for Revealing Protein Ratiometric Relationship Associated with EGFR–HER2 Heterodimerization in Living Cells
Xiaoxu Li, Yun Chen, *et al.*
JUNE 16, 2022
ANALYTICAL CHEMISTRY
READ

Get More Suggestions >

https://doi.org/10.1021/jacs.2c05203
J. Am. Chem. Soc. 2022, 144, 17432−17440